4. Huo TI, Wu JC, Lee PC, Chau GY, Lui WY, Tsay SH, et al. Seroclearance of hepatitis B surface antigen in chronic carriers does not necessarily imply a good prognosis. Hepatology. 1998;28: 231–6.
5. Iloeje UH, Yang HI, Su J, Jen CL, You SL, Chen CJ. Predicting cirrhosis risk based on the level of circulating hepatitis B viral load. Gastroenterology. 2006;130:678–86.
6. Arase Y, Ikeda K, Suzuki F, Suzuki Y, Saitoh S, Kobayashi M, et al. Long-term outcome after hepatitis B surface antigen seroclearance in patients with chronic hepatitis B. Am J Med. 2006;119:71.e9–16.
7. Chen YC, Sheen IS, Chu CM, Liaw YF. Prognosis following spontaneous HBsAg seroclearance in chronic hepatitis B patients with or without concurrent infection. Gastroenterology. 2002;123: 1084–9.
8. Chu CM, Liaw YF. HBsAg seroclearance in asymptomatic carriers of high endemic areas: appreciably high rates during a long-term follow-up. Hepatology. 2007;45:1187–92.
9. Yuen MF, Wong DK, Fung J, Ip P, But D, Hung I, et al. HBsAg seroclearance in chronic hepatitis B in Asian patients: replicative level and risk of hepatocellular carcinoma. Gastroenterology. 2008;135:1192–9.
10. Suzuki F, Arase Y, Suzuki Y, Akuta N, Sezaki H, Seko Y, et al. Long-term efficacy of interferon therapy in patients with chronic hepatitis B virus infection in Japan. J Gastroenterol. 2012;47:814–22.
11. Kobayashi M, Suzuki F, Akuta N, Hosaka T, Sezaki H, Yatsuji H, et al. Loss of hepatitis B surface antigen from the serum of patients with chronic hepatitis treated with lamivudine. J Med Virol. 2007;79:1472–7.
12. Akuta N, Suzuki F, Suzuki Y, Sezaki H, Hosaka T, Someya T, et al. Favorable efficacy of long-term lamivudine therapy in patients with chronic hepatitis B: an 8-year follow-up study. J Med Virol. 2005;75:491–8.
13. Hosaka T, Suzuki F, Kobayashi M, Seko Y, Kawamura Y, Sezaki H, et al. Clearance of hepatitis B surface antigen during long-term nucleot(s)ide analog treatment in chronic hepatitis B: results from a nine-year longitudinal study. J Gastroenterol. 2012. doi:10.1007/s00535-012-0688-7.
14. Ahn SH, Park YN, Park JY, Chang HY, Lee JM, Shin JE, et al. Long-term clinical and histological outcomes in patients with spontaneous hepatitis B surface antigen seroclearance. J Hepatol. 2005;42:188–94.
15. Kim JH, Lee JH, Park SJ, Bae MH, Kim JH, Kim do Y, et al. Factors associated with natural seroclearance of hepatitis B surface antigen and prognosis after seroclearance: a prospective follow-up study. Hepatogastroenterology. 2008;55:578–81.
16. Liaw YF, Leung N, Kao JH, Piratvisuth T, Gane E, Han KH, et al. Asian-Pacific consensus statement on the management of chronic hepatitis B: a 2008 update. Hepatol Int. 2008;2:263–83.
17. Liu J, Yang HI, Lee MH, Lu SN, Jen CL, Wang LY, et al. Incidence and determinants of spontaneous hepatitis B surface antigen seroclearance: a community-based follow-up study. Gastroenterology. 2010;139:474–82.
18. Kato Y, Nakao K, Hamasaki K, Kato H, Nakata K, Kusumoto Y, et al. Spontaneous loss of hepatitis B surface antigen in chronic carriers, based on a long-term follow-up study in Goto Islands, Japan. J Gastroenterol. 2000;35:201–5.
19. McMahon BJ, Holck P, Bulkow L, Snowball M. Serologic and clinical outcomes of 1536 Alaska natives chronically infected with hepatitis B virus. Ann Intern Med. 2001;135:759–68.
20. Simonetti J, Bulkow L, McMahon BJ, Homan C, Snowball M, Negus S, et al. Clearance of hepatitis B surface antigen and risk of hepatocellular carcinoma in a cohort chronically infected with hepatitis B virus. Hepatology. 2010;51:1531–7.
21. Shiraki K, Yoshihara N, Sakurai M, Eto T, Kawana T. Acute hepatitis B in infants born to carrier mothers with the antibody to hepatitis B e antigen. J Pediatr. 1980;97:768–70.

Pathology

Pathology International 2013; **63**: 305–310 doi:10.1111/pin.12064

Original Article

Quantification of collagen and elastic fibers using whole-slide images of liver biopsy specimens

Tokiya Abe,[1] Akinori Hashiguchi,[1] Ken Yamazaki,[1] Hirotoshi Ebinuma,[2,3] Hidetsugu Saito,[2,3] Hiromitsu Kumada,[4] Namiki Izumi,[5] Naohiko Masaki[6] and Michiie Sakamoto[1]

Departments of [1]Pathology and [2]Internal Medicine, School of Medicine, and [3]Faculty of Pharmacy, Keio University, [4]Department of Gastroenterology, Toranomon Hospital, [5]Department of Gastroenterology and Hepatology, Musashino Red Cross Hospital, Tokyo and [6]The Research Center for Hepatitis and Immunology, National Center for Global Health and Medicine, Chiba, Japan

Histological evaluation of fibrosis after a liver biopsy is crucial for evaluating the pathology of patients with chronic liver disease. Previous studies have reported quantitative analyses of fibrosis using images of collagen-stained sections. However, analysis of these studies requires manual selection of the region of interest. In addition, the quantification of elastic fibers is not considered. The present study was conducted in order to measure both the collagen and elastic fiber area ratios using Elastica van Gieson-stained whole-slide images (WSIs) of liver biopsy specimens. High-resolution WSIs provide precise color classification, enabling accurate detection of even fine collagen and elastic fibers. To minimize the influence of pre-existing fibrous tissue, median area ratios of the collagen and elastic fibers were independently calculated from the image tiles of the WSIs. These median area ratios were highly concordant with area ratios after the pre-existing fibrous tissues were manually trimmed from the WSI. Further, these median area ratios were correlated with liver stiffness as measured by transient elastography (collagen: $r = 0.73$ [$P < 0.01$], elastic: $r = 0.53$ [$P < 0.01$]). Our approach to quantifying liver fibrosis will serve as an effective tool to evaluate liver diseases in routine practice.

Key words: collagen, computer-assisted image analysis, elastin, elastography, liver fibrosis, whole-slide image

Evaluation of liver fibrosis in patients with chronic liver disease is crucial for understanding the disease state, predicting prognosis and selecting the appropriate treatment.[1,2] Although the efficacy of biochemical methods[3–6] and transient elastography for measuring liver stiffness[7] has been demonstrated, histopathological evaluation of liver biopsy specimens remains the gold standard. At present, histopathological evaluation of fibrosis using liver biopsy specimens is performed by a pathologist who stages specimens by identifying the location, degree and pattern of fibrosis, presence of architectural distortion, and regenerative nodule formation. This staging is completely dependent on the experience of the observer, and there is intra- as well as inter-individual variation in this respect.[1] To overcome these issues, quantification by imaging analysis has been suggested for evaluating the degree of liver fibrosis.[8–17] In these studies, collagen fibers were extracted from the histological image of the liver biopsy specimen, and the area occupied by the fibers relative to the area of the entire tissue specimen was quantified as a ratio. However, most of the proposed quantification methods still need an observer to define the region of interest or trim pre-existing fibrous tissue such as skin, muscle, or a large blood vessel.[8–14] An increase in collagen deposition is involved in the progression of liver fibrosis. Deposition of elastic fibers is also reportedly increased, particularly in late stages of the disease.[18–21] Thus, evaluation of elastic as well as collagen fiber deposition is crucial for the accurate evaluation of fibrosis progression; however, to our knowledge, no method that simultaneously quantifies both fibers has been reported to date.

The whole-slide imaging system, which is popular in telepathology and education, enables an entire tissue section to be digitized at a high resolution within minutes and saved as a whole-slide image (WSI).[22–24] Once the WSI is stored as digital data, it is easy to obtain individual pixel color values, and WSIs can be used for several applications including morphometrical analysis.[25–28] The purpose of this study is to develop an effective method to quantify liver fibrosis using

Correspondence: Michiie Sakamoto, MD, PhD, Department of Pathology, School of Medicine, Keio University, 35 Shinanomachi, Shinjuku-ku, Tokyo 160-8582, Japan. Email: msakamot@z5.keio.jp

Received 24 January 2013. Accepted for publication 2 May 2013.

the WSIs of liver biopsy specimens. We established a method that simultaneously quantifies the collagen and elastic fiber area ratios in Elastica van Gieson (EVG)-stained liver biopsy tissue specimens. Further, the area ratios were compared with liver stiffness as measured by transient elastography. This method of quantifying liver fibrosis using WSIs may become important in the future as a technique for assisting with pathological diagnosis.

METHODS

Samples

Liver biopsy specimens were collected from 38 chronic viral hepatitis patients (37 with chronic hepatitis C virus, and one with chronic hepatitis B virus) from four medical facilities. After obtaining the informed consent, we measured the liver stiffness by using FibroScan (Echo-Sens, Paris, France). The stiffness of the right lobe of the liver was measured by placing a probe tip into the intercostal space at a depth of 2.5–6 cm from the skin surface. Liver stiffness was measured 10 times, and the median value of these 10 measurements was used for each patient.

EVG staining

The liver biopsy specimens were formalin-fixed and paraffin-embedded. The specimens were then sliced to a thickness of 3 μm and stained with EVG. A WSI of each specimen was acquired using the NanoZoomer 2.0HT (Hamamatsu Photonics K.K., Hamamatsu, Japan) at a × 20 objective lens equivalent to 0.46 μm/pixel.

Quantification of fibrosis using WSI analysis

The WSI pixels were classified into five classes corresponding to four tissue components: collagen fibers, elastic fibers, nucleus, cytoplasm, and one non-tissue component (i.e. glass slide). The training data points, which were extracted from the portal and periportal areas in the WSI, were sampled for at least 30 points for each class. The color distributions of the five classes were analyzed in RGB color space, wherein the color analyses were done for all specimens. Subsequently, a quadratic discriminant function based on the color distribution[29] was applied in order to label each WSI pixel appropriately.

The area ratio of each tissue component is the sum of pixels for each tissue component divided by the total number of pixels of the four tissue components. The median area ratios of collagen and elastic fibers were also calculated. An image-processing program was developed using MATLAB (The MathWorks, Inc., Natick, MA, USA) for image analysis.

Statistical analysis

Relationships between measurement values were analyzed using the Spearman's rank correlation coefficient test. All *P*-values were two-tailed, and values less than 0.05 were considered statistically significant. Analyses were carried out using SPSS software (version 19.0; SPSS Inc., Chicago, IL, USA).

RESULTS

The evaluated liver biopsy specimens had an average length of 16.3 mm (SD = 3.2 mm) and an average width of 1.0 mm (SD = 0.3 mm). This is equivalent to an average of 77 mega-pixels (SD = 36 mega-pixels) in WSIs. The time required for analysis was approximately 6.3 min (SD = 3.3 min) per biopsy specimen.

Color classification of EVG-stained tissue specimens

The training data points for five classes were from the portal and periportal areas on the WSI of EVG-stained liver biopsy specimens (Fig. 1a). The extracted training data points were plotted in RGB color space (Fig. 1b). Five classes of the data points in all liver biopsy specimens were individually distinguishable in the three-dimensional color space. The composition of the color distribution of the five classes was different among the biopsy specimens, therefore, the quadratic discriminant function was designed based on the training data points in each liver biopsy specimen and applied to determine the color classification of the pixels. As a result, every pixel on the WSIs of all liver biopsy specimens was successfully labeled in the appropriate classes (Figs S1,S2). Figure 2 shows that even fine collagen and elastic fibers could be extracted from portal and periportal areas.

Measurements of the area ratios of tissue components on WSIs

The area ratio of each tissue component could be calculated from the labeled pixels. The average area ratios of collagen, elastic fibers, nucleus and cytoplasm in all biopsy specimens were 11.3% (SD = 5.1%), 3.8% (SD = 2.7%), 11.8% (SD = 5.0%) and 73.1% (SD = 8.7%), respectively. Representative WSIs and classification results of liver biopsy specimens with mild fibrosis and severe fibrosis are shown in

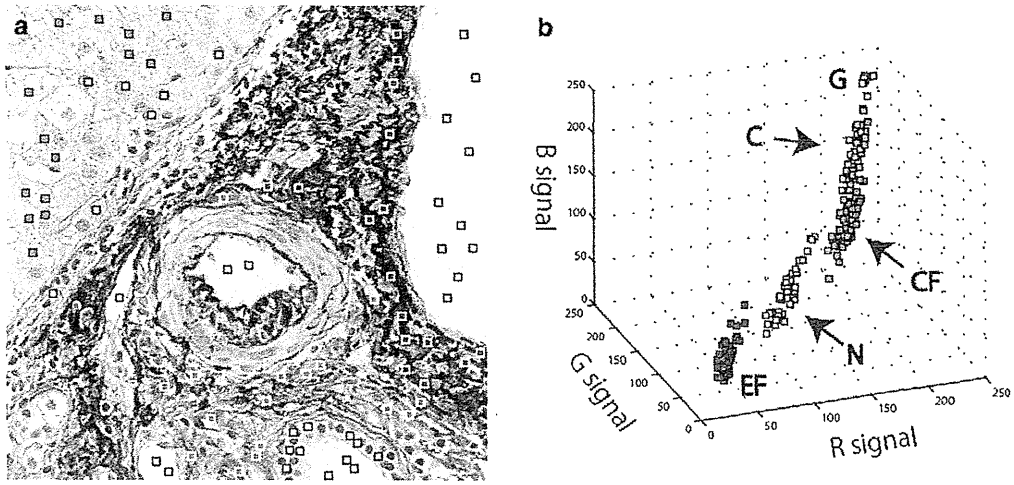

Figure 1 Sampling and color distribution. (**a**) Colored squares indicate training data points for five classes in the portal and periportal area (250 × 250 μm²). (**b**) Color distribution of the data points in RGB color space. Each color represents a class: collagen fiber (CF), red; elastic fibers (EF), blue; cell nuclei (N), yellow; cytoplasm (C), green; glass slide (G), white.

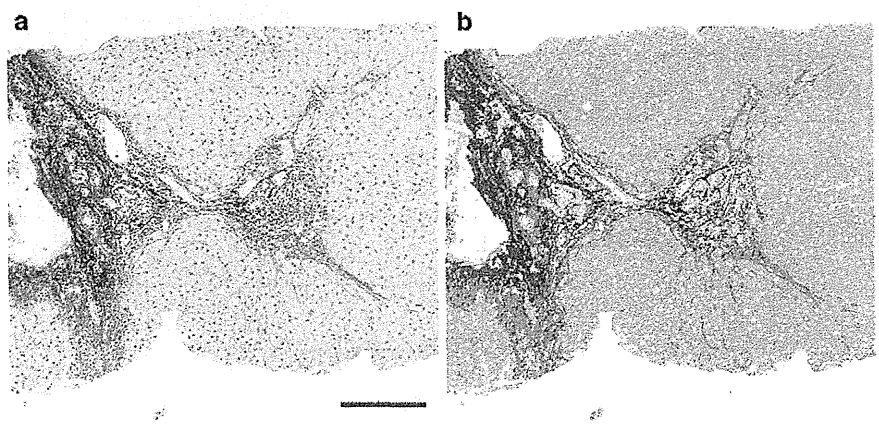

Figure 2 Color image and classification result in the portal and periportal areas (1 × 1 mm²). In the color classification result, collagen fibers, elastic fibers, nuclei, cytoplasm, and glass slide were red, blue, yellow, green, and white, respectively. Scale bar, 0.2 mm.

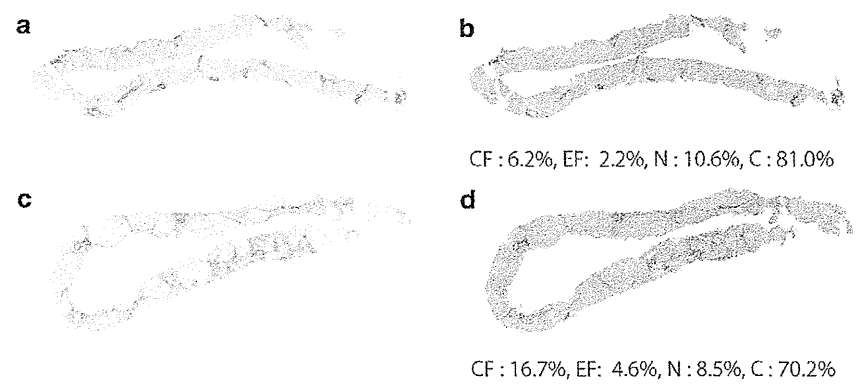

Figure 3 Measurements of area ratio on the whole-slide image. Representative whole slide images (WSIs) and classification results of liver biopsy specimen with mild fibrosis (**a,b**) and with severe fibrosis (**c,d**). The percentage indicates area ratio of each tissue component.

Figure 3a–d. The area ratios of collagen, elastic fibers, nucleus, and cytoplasm were 6.2%, 2.2%, 10.6%, and 81.0%, respectively, for mild fibrosis. The area ratios for severe fibrosis were 16.7%, 4.6%, 8.5%, and 70.2%, respectively. The area ratios of collagen as well elastic fibers were higher for patients with severe fibrosis than for those with mild fibrosis.

Median area ratios of collagen and elastic fibers

Previous papers reported that pre-existing fibrous tissue, such as muscle and large blood vessels (enclosed by the dotted line in Fig. 4a), should be trimmed from the WSI prior to implementing image analysis.[8,9] The measurements show that without trimming the pre-existing fibrous tissue,

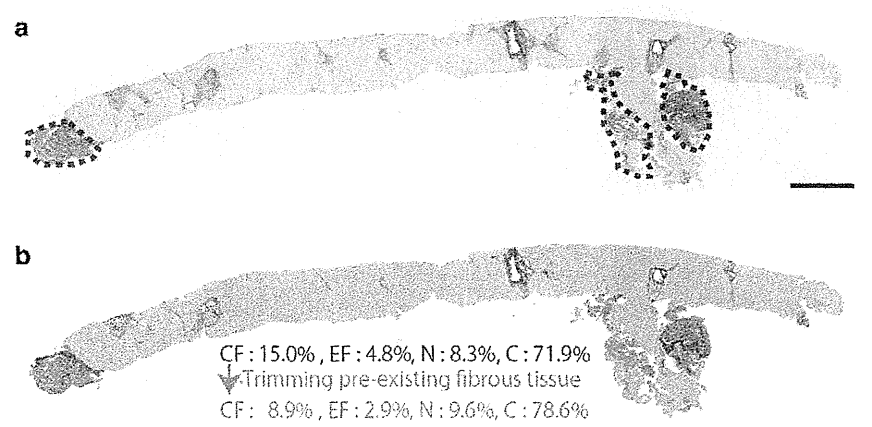

c												
			4.5	7.1	4.0	2.6	15.4	7.4	8.0	7.5	3.9	
	12.0	16.3	10.2	3.8	2.1				26.6	45.0	5.7	
57.2	29.3		Median area ratio of collagen fiber = 8.0 %						29.9	24.8		

d												
			1.0	1.1	1.3	0.4	11.6	2.4	4.5	2.3	0.7	
	5.1	2.3	3.9	0.6	0.5				5.4	16.1	1.2	
21.1	12.6		Median area ratio of elatic fiber = 2.4 %						3.3	3.9		

Figure 4 Median area ratios of collagen and elastic fibers. (**a,b**) Whole-slide image (WSI) and classification result of the liver biopsy specimen with mild fibrosis. (**c,d**) Median area ratios of collagen and elastic fibers, respectively, when the classification result was divided into 1×1 mm^2. Black numbers indicate area ratios of each fiber for any tiles where the tissue area occupied at least 20% of the tile area. The red number was the median area ratio of each fiber. Scale bar, 1 mm.

Table 1 Correlation between the median area ratio and area ratio after trimming the pre-existing fibrous tissue from the whole slide image

Tile size (mm^2)	0.01^2	0.25^2	0.50^2	0.75^2	1.00^2	1.25^2	1.50^2
Spearman's rank correlation coefficient							
Collagen fiber	0.79**	0.94**	0.98**	0.97**	0.98**	0.95**	0.93**
Elastic fiber	0.59**	0.87**	0.93**	0.93**	0.95**	0.92**	0.88**

**$P < 0.01$.

the area ratios of collagen and elastic fibers were 15.0% and 4.8%, respectively. After trimming, the area ratios of collagen and elastic fibers were 8.9% and 2.9%, respectively (Fig. 4b).

We then calculated the median area ratios of collagen and elastic fibers from the image tiles of WSI (Fig. 4c,d). The WSI was divided into small tiles of 1×1 mm^2. Then area ratios of each fiber on any tile, where the tissue area occupied at least 20% of the tile area, was calculated. The median area ratios of collagen and elastic fibers were determined as 8.0% (Fig. 4c) and 2.4% (Fig. 4d), respectively.

In order to determine the appropriate tile size, correlation between the median area ratios in other tile sizes and the area ratio after trimming were evaluated for all 38 liver biopsy specimens (Table 1). When the tile size was 1×1 mm^2, the median area ratios of the fibers correlated with the area ratio after trimming most strongly.

Relationship between the area ratio of fiber and liver stiffness

Correlation between the median area ratio of each fiber and liver stiffness measured by transient elastography was evaluated (Fig. 5a,b). Liver stiffness correlated well with the median area ratios of both types of fibers using a tile size of 1×1 mm^2 (collagen fiber: $r = 0.73$ [$P < 0.01$]; elastic fiber: $r = 0.53$ [$P < 0.01$]), as well as the area ratios after trimming pre-existing fibrous tissue off from WSI (collagen fiber: $r = 0.73$ [$P < 0.01$], elastic fiber: $r = 0.51$ [$P < 0.01$]). Liver

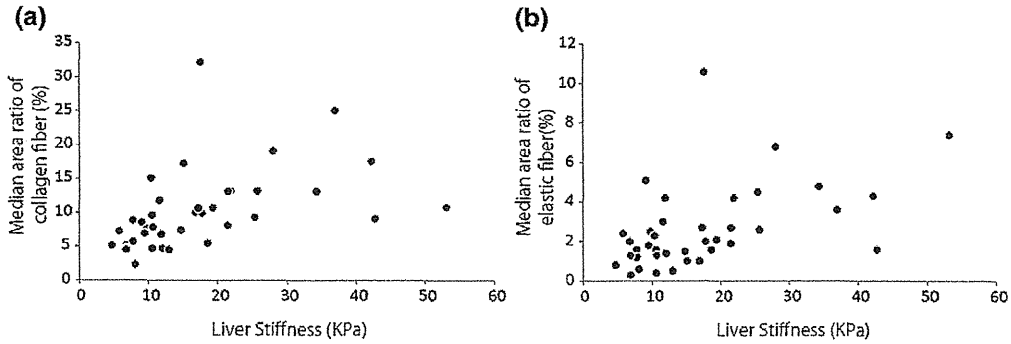

Figure 5 Scatter plot of liver stiffness by transient elastography versus median area ratios of (**a**) collagen and (**b**) elastic fibers. The tile size was 1×1 mm^2 when calculating the median area ratios of both fibers.

stiffness showed better correlation with the median area ratios of both fibers than with the area ratios including pre-existing fibrous tissue (collagen fiber: $r = 0.62$ [$P < 0.01$], elastic fiber: $r = 0.44$ [$P < 0.01$]).

DISCUSSION

Our color classification technique successfully labeled the WSI pixels of EVG-stained liver biopsy specimens in the appropriate classes (collagen, elastic fibers, nucleus, cytoplasm, and glass slide). Even fine collagen and elastic fibers, associated with chronic hepatitis, were accurately detected. Our results suggest that the precise recognition of tissue components in WSIs could identify not only portal fibrosis in patients with chronic viral hepatitis, but also fine pericellular fibrosis in those with alcoholic and non-alcoholic fatty liver diseases.

Pre-existing fibrous tissue such as skin, muscle and large blood vessel affects the accuracy of liver fibrosis measurements.[8] Previous studies have reported that the area ratio of collagen fiber was calculated after trimming pre-existing fibrous tissue from WSI.[8,9] Our study indicates that the trimming step could be avoided by calculating the median area ratios of collagen and elastic fibers from the image tiles of WSI. This approach can minimize the human factor and serve to establish an objective and automated quantification method. This type of image processing is one of the advantages of WSI analysis. We believe that more beneficial and useful algorithms will be developed in the near future.

Liver stiffness measured by transient elastography has been reported to correlate with the liver fibrosis stages.[7] Our results show that liver stiffness had a better correlation with the median area ratios of fibers than with the area ratios of fibers, including pre-existing fibrous tissue. This result suggests that the median area ratio of each fiber increases the correlation with liver stiffness and reflects the progression of liver fibrosis quantitatively. The liver stiffness, especially, correlated better with the median area ratio of collagen fiber than with the median area ratio of elastic fiber, probably due to an increase in elastic fiber in the late stages of the disease.[19–21] It is also possible that liver stiffness may relate to the width or density of fibrous septa.[30] However, we need to integrate other algorithms or densitometric method in order to measure those parameters and illuminate their relationships. The quantification of collagen and elastic fibers in a large number of cases would contribute to the understanding of the mechanism of fibrosis progression associated with chronic liver disease with different etiology, and would help to evaluate clinical usefulness.

In conclusion, a method for simultaneously quantifying collagen and elastic fibers was developed using WSIs of EVG-stained liver biopsy specimens. Median area ratios of collagen and elastic fibers obtained from the image tiles of WSIs were found to be correlated with liver stiffness measured by transient elastography. This enabled more accurate quantification of liver fibrosis than the area ratio of each fiber, including pre-existing fibrous tissue. Our approach of quantifying liver fibrosis will serve as a useful tool to effectively evaluate liver diseases in routine practice.

ACKNOWLEDGMENTS

This study was supported by the New Energy and Industrial Technology Development Organization (NEDO). The authors thank K. Effendi, M. Iwata, M. Takeichi, Y. Nagafuji, and Y. Hashimoto for technical assistance.

REFERENCES

1 The French METAVIR Cooperative Study Group. Intraobserver and interobserver variations in liver biopsy interpretation in patients with chronic hepatitis C. *Hepatology* 1994; **20**: 15–20.
2 Desmet VJ, Knodell RG, Ishak KG *et al.* Formulation and application of a numerical scoring system for assessing histological activity in asymptomatic chronic active hepatitis [Hepatology 1981; 1: 431–435]. *J Hepatol* 2003; **38**: 382–6.
3 Koda M, Matunaga Y, Kawakami M, Kishimoto Y, Suou T, Murawaki Y. FibroIndex, a practical index for predicting significant fibrosis in patients with chronic hepatitis C. *Hepatology* 2007; **45**: 297–306.

4 Forns X, Ampurdanes S, Llovet JM *et al.* Identification of chronic hepatitis C patients without hepatic fibrosis by a simple predictive model. *Hepatology* 2002; **36**: 986–92.
5 Wai CT, Greenson JK, Fontana RJ *et al.* A simple noninvasive index can predict both significant fibrosis and cirrhosis in patients with chronic hepatitis C. *Hepatology* 2003; **38**: 518–26.
6 Ngo Y, Munteanu M, Messous D *et al.* A prospective analysis of the prognostic value of biomarkers (FibroTest) in patients with chronic hepatitis C. *Clin Chem* 2006; **52**: 1887–96.
7 Ebinuma H, Saito H, Komuta M *et al.* Evaluation of liver fibrosis by transient elastography using acoustic radiation force impulse: Comparison with Fibroscan ®. *J Gastroenterol* 2011; **46**: 1238–48.
8 Standish RA, Cholongitas E, Dhillon A, Burroughs AK, Dhillon AP. An appraisal of the histopathological assessment of liver fibrosis. *Gut* 2006; **55**: 569–78.
9 Calvaruso V, Burroughs AK, Standish R *et al.* Computer-assisted image analysis of liver collagen: Relationship to Ishak scoring and hepatic venous pressure gradient. *Hepatology* 2009; **49**: 1236–44.
10 Goodman ZD, Becker RL Jr, Pockros PJ, Afdhal NH. Progression of fibrosis in advanced chronic hepatitis C: Evaluation by morphometric image analysis. *Hepatology* 2007; **45**: 886–94.
11 Goodman ZD, Stoddard AM, Bonkovsky HL *et al.* HALT-C Trial Group. Fibrosis progression in chronic hepatitis C: Morphometric image analysis in the HALT-C trial. *Hepatology* 2009; **50**: 1738–49.
12 Lazzarini AL, Levine RA, Ploutz-Snyder RJ, Sanderson SO. Advances in digital quantification technique enhance discrimination between mild and advanced liver fibrosis in chronic hepatitis C. *Liver Int* 2005; **25**: 1142–9.
13 McHutchison J, Goodman Z, Patel K *et al.*; Farglitizar Study Investigators. Farglitazar lacks antifibrotic activity in patients with chronic hepatitis C infection. *Gastroenterology* 2010; **138**: 1365–73. 1673 e1–2.
14 O'Brien MJ, Keating NM, Elderiny S *et al.* An assessment of digital image analysis to measure fibrosis in liver biopsy specimens of patients with chronic hepatitis C. *Am J Clin Pathol* 2000; **114**: 712–18.
15 Wright M, Thursz M, Pullen R, Thomas H, Goldin R. Quantitative versus morphological assessment of liver fibrosis: Semi-quantitative scores are more robust than digital image fibrosis area estimation. *Liver Int* 2003; **23**: 28–34.
16 Masseroli M, Caballero T, O'Valle F, Del Moral RM, Perez-Milena A, Del Moral RG. Automatic quantification of liver fibrosis: Design and validation of a new image analysis method: Comparison with semi-quantitative indexes of fibrosis. *J Hepatol* 2000; **32**: 453–64.
17 Hui AY, Liew CT, Go MY *et al.* Quantitative assessment of fibrosis in liver biopsies from patients with chronic hepatitis B. *Liver Int* 2004; **24**: 611–18.
18 Shikata T, Skai T. Elastogenesis in the liver. *Acta Pathol Jpn* 1974; **24**: 21–31.
19 Scheuer PJ, Maggi G. Hepatic fibrosis and collapse: Histological distinction by orecin staining. *Histopathology* 1980; **4**: 487–90.
20 Thung SN, Gerber MA. The formation of elastic fibers in livers with massive hepatic necrosis. *Arch Pathol Lab Med* 1982; **106**: 468–9.
21 Bedossa P, Lemaigre G, Paraf F, Martin E. Deposition and remodelling of elastic fibres in chronic hepatitis. *Virchows Arch A Pathol Anat Histopathol* 1990; **417**: 159–62.
22 Gilbertson JR, Ho J, Anthony L, Jukic DM, Yagi Y, Parwani AV. Primary histologic diagnosis using automated whole slide imaging: A validation study. *BMC Clin Pathol* 2006; **6**: 4.
23 Glatz-Krieger K, Glatz D, Mihatsch MJ. Virtual slides: High-quality demand, physical limitations, and affordability. *Hum Pathol* 2003; **34**: 968–74.
24 Weinstein RS, Graham AR, Richter LC *et al.* Overview of telepathology, virtual microscopy, and whole slide imaging: Prospects for the future. *Hum Pathol* 2009; **40**: 1057–69.
25 Diamond J, Anderson NH, Bartels PH, Montironi R, Hamilton PW. The use of morphological characteristics and texture analysis in the identification of tissue composition in prostatic neoplasia. *Hum Pathol* 2004; **35**: 1121–31.
26 Hashiguchi A, Hashimoto Y, Suzuki H, Sakamoto M. Using immunofluorescent digital slide technology to quantify protein expression in archival paraffin-embedded tissue sections. *Pathol Int* 2010; **60**: 720–25.
27 Puppa G, Risio M, Sheahan K *et al.* Standardization of whole slide image morphologic assessment with definition of a new application: Digital slide dynamic morphometry. *J Pathol Inform* 2011; **2**: 48.
28 Sertel O, Kong J, Shimada H, Catalyurek UV, Saltz JH, Gurcan MN. Computer-aided prognosis of neuroblastoma on whole-slide images: Classification of stromal development. *Pattern Recognit* 2009; **42**: 1093–103.
29 Gonzalez RC, Woods RE. Object recognition. In: Gonzalez RC, Woods RE, eds. *Digital Image Processing*, 3rd edn. Upper Saddle River, NJ: Pearson Prentice Hall, 2010; 896–9.
30 Zhang YG, Wang BE, Wang TL, Ou XJ. Assessment of hepatic fibrosis by transient elastography in patients with chronic hepatitis B. *Pathol Int* 2010; **60**: 284–90.

SUPPORTING INFORMATION

Additional Supporting Information may be found in the online version of this article at the publisher's web-site:

Figure S1 Whole slide images (WSIs) of liver biopsies from 38 chronic viral hepatitis patients.

Figure S2 Color classification results for WSIs.

CASE REPORT

Gut and Liver, Vol. 7, No. 2, March 2013, pp. 246-251

Transcatheter Arterial Chemotherapy with Miriplatin for Hepatocellular Carcinoma Patients with Chronic Renal Failure: Report of Three Cases

Norihiro Imai, Kenji Ikeda, Yuya Seko, Yusuke Kawamura, Hitomi Sezaki, Tetsuya Hosaka, Norio Akuta, Masahiro Kobayashi, Satoshi Saitoh, Fumitaka Suzuki, Yoshiyuki Suzuki, Yasuji Arase, and Hiromitsu Kumada

Department of Hepatology, Toranomon Hospital, Tokyo, Japan

Miriplatin is a novel lipophilic platinum complex that was developed to treat hepatocellular carcinoma (HCC). Although HCC patients frequently have coexisting chronic renal failure, little prospective data are available regarding the clinical toxicity of chemotherapeutic agents used to treat HCC patients with chronic renal failure. In a phase II study, the plasma concentration of total platinum in patients who received miriplatin was very low, and no severe renal toxicity caused by miriplatin injection was reported. Here, we present three cases of HCC with stage 4 chronic renal failure who received transcatheter arterial chemotherapy with miriplatin. All cases were male, ages 72, 84, and 83 years, and had serum creatinine levels of 2.3, 1.6, and 1.9 mg/dL, respectively. Their estimated glomerular filtration rates were 21.9, 20.3, and 22.2 mL/min, respectively. All cases were treated for unresectable HCC with transcatheter arterial chemotherapy with miriplatin. No serious adverse events were observed, and serum creatinine levels did not elevate, even in the patient who experienced renal failure caused by cisplatin administration. These results might suggest that transcatheter arterial chemotherapy with miriplatin can be safely used in HCC patients with chronic renal failure. **(Gut Liver 2013;7:246-251)**

Key Words: Miriplatin; Chronic renal failure; Hepatocellular carcinoma

INTRODUCTION

Hepatocellular carcinoma (HCC) is one of the most common malignant diseases worldwide.[1] Since curative therapies, including resection, liver transplantation, and percutaneous ablation (percutaneous ethanol injection and radiofrequency ablation [RFA]) are applicable in only 30% to 40% of HCC patients, transcatheter arterial chemoembolization (TACE) has been recognized as an effective palliative treatment option for patients with advanced HCC.[2-7] HCC patients frequently have coexisting cirrhosis, which is a predisposing factor for the development of renal dysfunction due to intravascular volume depletion, inadequate renal vasoconstriction, and hyperaldosteronism.[8-13]

Little prospective data are available regarding the clinical toxicity of chemotherapeutic agents used to treat HCC patients with chronic renal failure. Although cisplatin is an effective anticancer drug that is widely used for the treatment of many malignancies, including HCC, it is associated with significant nephrotoxicity, particularly in patients with chronic renal failure.[2,7] Miriplatin is a novel cisplatin derivative containing platinum with a high affinity for the iodized ethyl ester of fatty acids of poppyseed oil (Lipiodol Ultra-fluide; Laboratoire Guerbet, Aulnay-Sous-Bois, France) that is used in TACE. Clinical trials have demonstrated that miriplatin is effective in the treatment of HCC.[14-19]

In a Phase II HCC study, the plasma concentration of total platinum in patients receiving miriplatin was very low, and no severe renal toxicity caused by miriplatin injection was reported.[17] Here we present three cases of HCC with stage 4 chronic renal failure who received transcatheter arterial chemotherapy with miriplatin.[20]

CASE REPORTS

1. Case 1

A 72-year-old man with HCC, liver cirrhosis, and diabetic nephropathy had undergone RFA four times and TACE three times over 5 years. As shown in Fig. 1, a computed tomography (CT) scan of the liver revealed multiple HCCs (tumor size, 15 to 34 mm; tumor number, three; stage, T2N0M0). The serum creati-

Correspondence to: Norihiro Imai
Department of Hepatology, Toranomon Hospital, 2-2-2 Toranomon, Minato-ku, Tokyo 105-8470, Japan
Tel: +81-3-3588-1111, Fax: +81-3-3582-7068, E-mail: norihiro.imai@gmail.com
Received on February 18, 2011. Revised on April 29, 2011. Accepted on June 12, 2011.
pISSN 1976-2283 eISSN 2005-1212 http://dx.doi.org/10.5009/gnl.2013.7.2.246

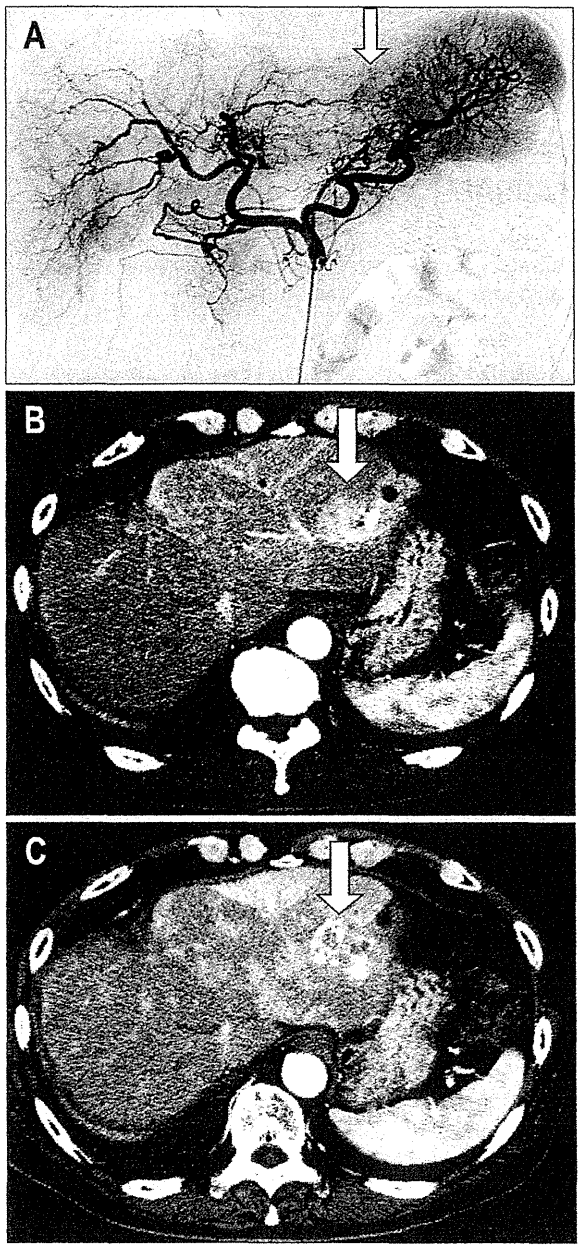

Fig. 1. Case 1. A 72-year-old man with unresectable hepatocellular carcinoma (HCC) who received transcatheter arterial chemoembolization (TACE) with miriplatin. (A) Abdominal angiography showed multiple HCCs (arrow). (B) Computed tomography (CT) showed multiple HCCs (arrow). (C) CT performed 1 month after TACE. The lesions revealed accumulations of lipiodol (arrow). Treatment efficacy was assessed as a partial response.

nine level was 2.3 mg/dL, and the estimated glomerular filtration rate (GFR) was 21.9 mL/min (Table 1).[21]

The patient was hydrated through a peripheral line. The femoral artery was catheterized under local anesthesia, and catheter was inserted superselectively into the hepatic artery that supplied the target tumor, for injection of the miriplatin/lipiodol suspension and 1 mm gelatin particles (1 mm-Gelpart; Nippon Kayaku, Tokyo, Japan). Miriplatin/lipiodol suspension was administrated slowly under careful fluoroscopic guidance. The dose of miriplatin/lipiodol was determined according to tumor size and the degree of liver dysfunction. The patient received TACE with miriplatin (miriplatin 50 mg, lipiodol 2.5 mL, and 1 mm-Gelpart were injected from both the right and left hepatic arteries). Therapy was well tolerated, and the patient's weight and serum creatinine level remained stable after treatment (Fig. 2). Major side effects included grade 1 fever, elevated blood glucose, and grade 1 nausea, which all resolved within 1 week (the National Cancer Institute's Common Terminology Criteria for Adverse Events [CTCAE] version 4.0). Treatment efficacy was assessed 1 month after treatment. Partial response (modified response evaluation criteria in solid tumors, mRECIST) was achieved in all target lesions.[22]

The patient was received two times TACE with miriplatin at intervals of 4 months after the first administration (second and third dosage of miriplatin were 120 mg and dosage of lipiodol were 6 mL). The patient's weight and serum creatinine level still remained stable after repeat injection of miriplatin (serum creatinine level was 2.2 mg/dL after third TACE with miriplatin). Stable disease (mRECIST) was achieved in all target lesions after third TACE with miriplatin.

2. Case 2

An 84-year-old man with HCC, liver cirrhosis, and chronic renal failure had undergone RFA three times and TACE six times over 10 years. As shown in Fig. 3, a CT scan of the liver showed multiple HCCs (tumor size, 12 to 55 mm; tumor number, six; stage, T3N0M0). The serum creatinine level was 1.6 mg/dL, and the estimated GFR was 20.3 mL/min (Table 1).

The patient was hydrated through a peripheral line. The femoral artery was catheterized under local anesthesia, and catheter was inserted superselectively into the hepatic artery that supplied the target tumor, for injection of the miriplatin/lipiodol suspension. Miriplatin/lipiodol suspension was administrated slowly under careful fluoroscopic guidance. The dose of miriplatin/lipiodol was determined according to tumor size and the degree of liver dysfunction.

The patient received transcatheter arterial chemotherapy with miriplatin (miriplatin 50 mg and lipiodol 2.5 mL were injected from both the right and left hepatic arteries). Therapy was well tolerated, and the patient's weight and serum creatinine level remained stable after treatment (Fig. 2). The major side effect of treatment was grade 1 fever, which resolved within 1 week (CTCAE version 4.0). Treatment efficacy was assessed 2 months after therapy. Stable disease (mRECIST) was achieved in all target lesions.

3. Case 3

An 83-year-old man with HCC, liver cirrhosis, hypertension,

Table 1. Patient Characteristics

Characteristic	Case 1	Case 2	Case 3
Age	72	84	83
Gender	Male	Male	Male
Height, cm	159	160	162
Weight, kg	58	47	57
Serum creatinine, mg/dL*	2.3	1.6	1.9
Estimated GFR1, mL/min†	21.9	20.3	22.2
Estimated GFR2, mL/min‡	22.8	32.5	27.0
Etiology	HCV	HCV	HBV
Child-Pugh score	A (6)	A (5)	A (5)
ICG-R15, %	16	13	4
Underlying disease that caused renal failure	Diabetic nephropathy	Chronic glomerulonephritis	Cisplatin induced renal failure
Tumor no.	3	6	40
Maximum tumor size, mm	34	55	39
Cancer stage (TNM)	II (T2N0M0)	III (T3N0M0)	II (T2N0M0)
Dosage of miriplatin, mg	100	100	70
Dosage of lipiodol, mL	5	5	3.5
Use of gelatin sponge particles	Yes	No	Yes
Contrast medium, mL	Iomeprol 60	Iomeprol 50	Iomeprol 190
Use of hydration therapy after miriplatin infusion	Yes	Yes	Yes

GFR, glomerular filtration rate; HCV, hepatitis C virus; HBV, hepatitis B virus; ICG-R15, indocyanine green retention rate at 15 minutes.
*Enzymatic method; †Cockcroft and Gault formula; ‡Japanese equation for estimating GFR.

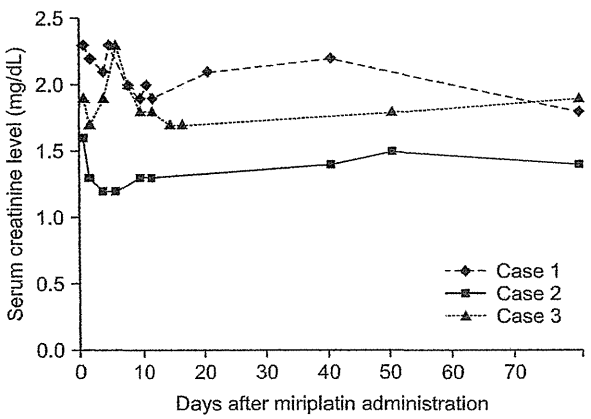

Fig. 2. Serum creatinine level after miriplatin administration in the three cases.

and renal failure that had been caused by cisplatin administration had undergone TACE nine times over 4 years. As shown in Fig. 4, a magnetic resonance imaging scan of the liver revealed multiple HCCs (tumor size, 5 to 39 mm; tumor number, 40; stage, T2N0M0). The patient's serum creatinine level was 1.9 mg/dL, and the estimated GFR was 22.2 mL/min (Table 1).

The patient was hydrated through a peripheral line. The femoral artery was catheterized under local anesthesia, and catheter was inserted superselectively into the hepatic artery that supplied the target tumor, for injection of the miriplatin/lipiodol suspension and 1 mm-Gelpart. Miriplatin/lipiodol suspension was administrated slowly under careful fluoroscopic guidance. The dose of miriplatin/lipiodol was determined according to tumor size and the degree of liver dysfunction.

The patient received TACE with miriplatin (miriplatin 30 mg, lipiodol 1.5 mL, and 1 mm-Gelpart were injected from the right and left hepatic arteries, and miriplatin 10 mg and lipiodol 0.5 mL were injected from the right inferior phrenic artery). Therapy was well tolerated, and the patient's weight and serum creatinine level remained stable after treatment (Fig. 2). Major side effects included grade 1 fever and grade 1 nausea, both of which resolved within 1 week (CTCAE version 4.0). Treatment efficacy was assessed 3 months after therapy. Stable disease (mRECIST) was achieved in all target lesions.

DISCUSSION

Various anticancer drugs, such as doxorubicin hydrochloride, epirubicin hydrochloride, mytomycin C, cisplatin, and neocarzinostatin, have been used at TACE agents for the treatment of HCC. However, the most effective and least toxic TACE protocol for HCC has yet to be identified.

Miriplatin is a novel lipophilic cisplatin derivative that can be suspended in lipiodol and used for transcatheter arterial che-

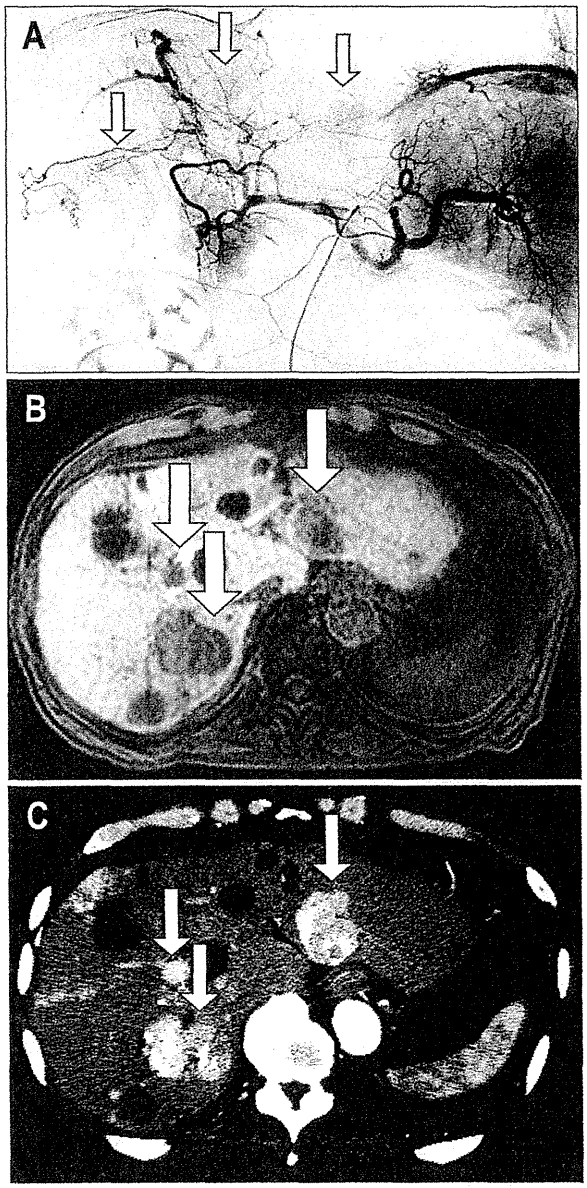

Fig. 3. Case 2. An 84-year-old man with unresectable hepatocellular carcinoma (HCC) who received transcatheter arterial chemotherapy with miriplatin. (A) Abdominal angiography showed multiple HCCs (arrows). (B) Magnetic resonance imaging (hepatobiliary phase) showed multiple HCCs (arrows). (C) Computed tomography performed 2 months after transcatheter arterial chemotherapy with miriplatin. The lesions showed accumulations of lipiodol (arrows). The treatment efficacy was assessed as a stable disease.

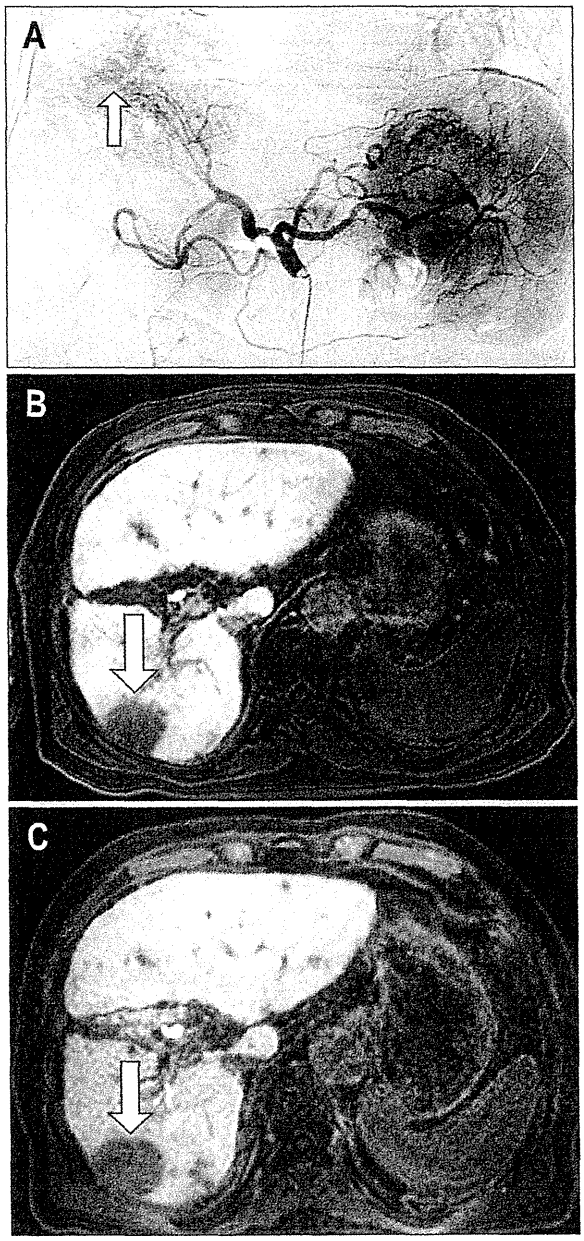

Fig. 4. Case 3. An 83-year-old man with unresectable hepatocellular carcinoma (HCC) who received transcatheter arterial chemoembolization (TACE) with miriplatin. (A) Abdominal angiography showed multiple HCCs (arrow). (B) Gadolinium ethoxybenzyl diethylenetriamine pentaacetic acid (Gd-EOB-DTPA) enhanced magnetic resonance imaging (MRI; hepatobiliary phase) showed multiple HCCs (arrow). (C) Gd-EOB-DTPA enhanced MRI performed 3 months after TACE. The lesions showed accumulations of lipiodol (arrow). The treatment efficacy was assessed as a stable disease.

motherapy of advanced HCC. It is one of the platinum agents, although hydration after administration is not necessary of its weak renal toxicity.

Various types of resistance to therapy can occur during repetition of TACE. Platinum derivatives are frequently administered to patients with advanced HCC that is unresponsive to anthracycline and antibiotic drugs.[23]

Miriplatin was developed as a lipophilic platinum complex in an effort to produce a superior antitumor effect in HCC with lower toxicity compared to cisplatin. Miriplatin-lipiodol suspension is a stable colloidal emulsion that is deposited within HCC tumors, where it gradually releases active derivatives of miripla-

tin.

According to pharmacokinetic studies, the plasma concentration of total platinum in patients treated with miriplatin is much lower than that after administration in patients administered intra-arterial cisplatin: the Cmax is approximately 300-fold lower and the Tmax roughly 500-fold longer than the corresponding values for intra-arterial cisplatin.[17] Theoretically, therefore, it can be administered even in patients of advanced HCC patients with chronic renal failure if visceral angiography can be performed.

Clinical trials have shown that miriplatin is effective for the treatment of HCC, but the safety and efficacy of miriplatin has not been evaluated in HCC patients with chronic renal failure.[16,17] Herein we presented three HCC cases with stage 4 chronic renal failure who received transcatheter arterial chemotherapy with miriplatin. In all three cases, no serious adverse events were observed, and serum creatinine level did not increase, even in the patient who had experienced renal failure due to cisplatin administration (Fig. 2). Repeated injection of miriplatin appears to be also safe in HCC patients with chronic renal failure.

The present results might suggest that transcatheter arterial chemotherapy with miriplatin can be safely used in HCC patients with chronic renal failure. A prospective study is required to assess the most effective, least nephrotoxic anticancer agent among the various platinum derivatives. Miriplatin appears to be a promising agent for HCC patients with chronic renal failure.

CONFLICTS OF INTEREST

The following authors have received honoraria (lecture fee) from Dainippon Sumitomo Pharma Co., Ltd., Osaka, Japan; Hiromitsu Kumada, MD, Kenji Ikeda, MD, Yasuji Arase, MD, Yoshiyuki Suzuki, MD, Fumitaka Suzuki, MD, and Norio Akuta, MD.

REFERENCES

1. Parkin DM, Bray F, Ferlay J, Pisani P. Global cancer statistics, 2002. CA Cancer J Clin 2005;55:74-108.
2. Kamada K, Nakanishi T, Kitamoto M, et al. Long-term prognosis of patients undergoing transcatheter arterial chemoembolization for unresectable hepatocellular carcinoma: comparison of cisplatin lipiodol suspension and doxorubicin hydrochloride emulsion. J Vasc Interv Radiol 2001;12:847-854.
3. Camma C, Schepis F, Orlando A, et al. Transarterial chemoembolization for unresectable hepatocellular carcinoma: meta-analysis of randomized controlled trials. Radiology 2002;224:47-54.
4. Ikeda M, Maeda S, Shibata J, et al. Transcatheter arterial chemotherapy with and without embolization in patients with hepatocellular carcinoma. Oncology 2004;66:24-31.
5. Takayasu K, Arii S, Ikai I, et al. Prospective cohort study of transarterial chemoembolization for unresectable hepatocellular carcinoma in 8510 patients. Gastroenterology 2006;131:461-469.
6. Marelli L, Stigliano R, Triantos C, et al. Transarterial therapy for hepatocellular carcinoma: which technique is more effective? A systematic review of cohort and randomized studies. Cardiovasc Intervent Radiol 2007;30:6-25.
7. Ikeda M, Maeda S, Ashihara H, Nagahama H, Tanaka M, Sasaki Y. Transcatheter arterial infusion chemotherapy with cisplatin-lipiodol suspension in patients with hepatocellular carcinoma. J Gastroenterol 2010;45:60-67.
8. Laragh JH, Cannon PJ, Bentzel CJ, Sicinski AM, Meltzer JI. Angiotensin Ii, Norepinephrine, and renal transport of electrolytes and water in normal man and in cirrhosis with ascites. J Clin Invest 1963;42:1179-1192.
9. Cardenas A, Ginès P, Uriz J, et al. Renal failure after upper gastrointestinal bleeding in cirrhosis: incidence, clinical course, predictive factors, and short-term prognosis. Hepatology 2001;34(4 Pt 1):671-676.
10. Moreau R, Lebrec D. Acute renal failure in patients with cirrhosis: perspectives in the age of MELD. Hepatology 2003;37:233-243.
11. Huo TI, Wu JC, Lee PC, Chang FY, Lee SD. Incidence and risk factors for acute renal failure in patients with hepatocellular carcinoma undergoing transarterial chemoembolization: a prospective study. Liver Int 2004;24:210-215.
12. Huo TI, Wu JC, Huang YH, et al. Acute renal failure after transarterial chemoembolization for hepatocellular carcinoma: a retrospective study of the incidence, risk factors, clinical course and long-term outcome. Aliment Pharmacol Ther 2004;19:999-1007.
13. Hsu CY, Huang YH, Su CW, et al. Renal failure in patients with hepatocellular carcinoma and ascites undergoing transarterial chemoembolization. Liver Int 2010;30:77-84.
14. Maeda M, Uchida NA, Sasaki T. Liposoluble platinum(II) complexes with antitumor activity. Jpn J Cancer Res 1986;77:523-525.
15. Kishimoto S, Ohtani A, Fukuda H, Fukushima S, Takeuchi Y. Relation between intracellular accumulation and cytotoxic activity of cis-[((1R, 2R)-1, 2-cyclohexanediamine-N, N')bis(myristato)] platinum(II) suspended in Lipiodol. Biol Pharm Bull 2003;26:683-686.
16. Fujiyama S, Shibata J, Maeda S, et al. Phase I clinical study of a novel lipophilic platinum complex (SM-11355) in patients with hepatocellular carcinoma refractory to cisplatin/lipiodol. Br J Cancer 2003;89:1614-1619.
17. Okusaka T, Okada S, Nakanishi T, Fujiyama S, Kubo Y. Phase II trial of intra-arterial chemotherapy using a novel lipophilic platinum derivative (SM-11355) in patients with hepatocellular carcinoma. Invest New Drugs 2004;22:169-176.
18. Hanada M, Baba A, Tsutsumishita Y, Noguchi T, Yamaoka T. Intra-hepatic arterial administration with miriplatin suspended in an oily lymphographic agent inhibits the growth of human hepatoma cells orthotopically implanted in nude rats. Cancer Sci 2009;100:189-194.
19. Hanada M, Baba A, Tsutsumishita Y, et al. Intra-hepatic arterial

administration with miriplatin suspended in an oily lymphographic agent inhibits the growth of tumors implanted in rat livers by inducing platinum-DNA adducts to form and massive apoptosis. Cancer Chemother Pharmacol 2009;64:473-483.

20. K/DOQI clinical practice guidelines for chronic kidney disease: evaluation, classification, and stratification. Kidney Disease Outcome Quality Initiative. Am J Kidney Dis 2002;39(Suppl 2):S7-S245.
21. Matsuo S, Imai E, Horio M, et al. Revised equations for estimated GFR from serum creatinine in Japan. Am J Kidney Dis 2009;53:982-992.
22. Lencioni R, Llovet JM. Modified RECIST (mRECIST) assessment for hepatocellular carcinoma. Semin Liver Dis 2010;30:52-60.
23. Kawamura Y, Ikeda K, Hirakawa M, et al. Efficacy of platinum analogue for advanced hepatocellular carcinoma unresponsive to transcatheter arterial chemoembolization with epirubicin. Hepatol Res 2009;39:346-354.

Hepatology Research

Hepatology Research 2013; 43: 836–845 doi: 10.1111/hepr.12025

Original Article

Magnetic resonance laparoscopy: A new non-invasive technique for the assessment of chronic viral liver disease

Suguru Ogura, Satoshi Saitoh, Yusuke Kawamura, Hitomi Sezaki, Tetsuya Hosaka, Norio Akuta, Masahiro Kobayashi, Fumitaka Suzuki, Yoshiyuki Suzuki, Yasuji Arase, Kenji Ikeda and Hiromitsu Kumada

Department of Hepatology, Toranomon Hospital, Tokyo, Japan

Aim: Laparoscopy-guided liver biopsy is the most accurate method for assessing liver fibrosis but have several limitations. We designed a non-invasive method, called magnetic resonance laparoscopy (MRL), based on gadolinium-ethoxybenzyl-diethylenetriamine pentaacetic acid-enhanced magnetic resonance imaging, to assess liver fibrosis in patients with chronic hepatitis B and C virus.

Methods: We prospectively analyzed 49 patients with normal liver and 353 patients with chronic viral hepatitis, laparoscopic liver biopsy was performed on 109 patients and 244 patients were diagnosed as having liver cirrhosis clinically. The MRL findings of the liver surface were classified into three categories: (i) smooth (essentially smooth surface of the entire liver or with limited areas of depression); (ii) partially irregular (several interconnected depressions on the surface mainly in the left lobe of the liver); and (iii) diffusely irregular (nodules present on the liver surface). Patients with diffusely irregular liver surface was diagnosed as liver cirrhosis.

Results: The liver surface changed with the progression of liver fibrosis from smooth, partially irregular to diffusely irregular, irrespective of viral type. The sensitivity, specificity, positive and negative predictive values for the diagnosis of cirrhosis according to the surface findings on MRL were 96%, 100%, 95% and 95%, respectively. The cirrhotic liver showed: (i) disappearance of impression of the right ribs; (ii) enlargement of the lateral segment; and (iii) atrophy of the right lobe according to Child–Pugh classification.

Conclusion: Our data indicated that MRL is a potentially useful non-invasive examination for evaluation of liver fibrosis associated with viral hepatitis.

Key words: chronic hepatitis, gadolinium-ethoxybenzyl-diethylenetriamine pentaacetic acid, laparoscopy, multiple resonance imaging, multiple resonance laparoscopy

INTRODUCTION

HEPATITIS C VIRUS (HCV) and hepatitis B virus (HBV) are common causes of chronic liver disease worldwide and often lead to liver cirrhosis and hepatocellular carcinoma (HCC).[1–7] The prognosis and clinical management of chronic liver diseases are highly dependent on the extent of liver fibrosis, as complications mainly occur in patients in the advanced stages. Therefore, accurate diagnosis of the extent of fibrosis is needed.

A definite diagnosis of chronic liver disease is established by histological examination of a biopsy specimen and by visualization of the liver surface at laparoscopy.[8–10] Laparoscopy-guided liver biopsy is considered the most accurate method for the diagnosis of liver disease, especially liver cirrhosis.[11,12] However, the use of laparoscopy as a diagnostic tool in liver has diminished over the past decade,[13,14] probably due to problems associated with safety and complexity compared with ultrasound-guided biopsy. Thus, ultrasound-guided liver biopsy is currently the gold standard in assessing liver histology. However, liver biopsy is also associated with at least a few problems even when performed by experienced hepatologists. In fact, obtaining a liver biopsy is an invasive procedure and associated sometimes with life-threatening complications.[15,16] Furthermore, sampling errors and intra- and interobserver variability may lead to over- or underestimation of fibrosis.[17–19]

Owing to the invasiveness of the biopsy procedure and its associated possible complications, the

Correspondence: Dr Satoshi Saitoh, Department of Hepatology, Toranomon Hospital, 2-2-2 Toranomon, Minato-ku, Tokyo 105-0001, Japan. Email: sa3110@f2.dion.ne.jp
Received 27 October 2011; revision 1 November 2012; accepted 11 November 2012.

development of alternative non-invasive methods to characterize the condition of the liver is highly desirable. Non-invasive approaches to assess histology in patients with chronic liver disease include clinical symptoms and signs, routine laboratory tests, serum markers of fibrosis and inflammation, quantitative assays of liver function, and radiologic imaging studies.[20–31] Although laparoscopy is more invasive than percutaneous liver biopsy, some studies reported that laparoscopy was more accurate than liver biopsy in the diagnosis of cirrhosis and prediction of HCC in patients with chronic viral hepatitis.[12,32,33] However, due to its invasive nature, other non-invasive substitute techniques of laparoscopy are required.

Gadolinium-ethoxybenzyl-diethylenetriamine pentaacetic acid (Gd-EOB-DTPA) is a liver-specific contrast medium used for multiple resonance imaging (MRI). A bolus injection of Gd-EOB-DTPA allows the evaluation of tumor vascularity in a manner similar to evaluation with Gd-DTPA. Furthermore, this contrast medium accumulates in normally functioning hepatocytes in the hepatobiliary phase, which begins 20 min after injection, and enhances the liver parenchyma. While normally functioning hepatocytes are enhanced in hepatobiliary phase, tumors appear as hypointense lesions because they lack normally functioning hepatocytes.[34,35] Based on these features, we devised multiple resonance laparoscopy (MRL), which includes reconstructed 3-D images obtained from hepatobiliary phase images of Gd-EOB-DTPA-enhanced MRI, to visualize the liver surface. The aim of this study was to assess the utility of this technique as a substitute for laparoscopy and its usefulness for assessment of chronic liver disease.

METHODS

Patients

THIS STUDY INCLUDED 49 patients who each had a small solitary hemangioma with normal liver and underwent Gd-EOB-DTPA-enhanced MRI. They consisted of 29 women and 20 men with a median age of 55 years (range, 32–70). The inclusion criteria were: (i) body mass index within the normal range (median, 21; range, 17–24); (ii) aspartate aminotransferase (AST) and alanine aminotransferase (ALT) within the normal range (median, 15 IU/L; range, 8–24 IU/L); (iii) negative for HCV RNA and hepatitis B surface antigen (HBsAg); (iv) maximum diameter of hemangioma less than 15 mm; (v) daily alcohol intake less than 10 mg/day; and (vi) absence of fatty liver as confirmed by ultrasonography. This study also included 101 hepatitis B patients and 252 hepatitis C patients who underwent Gd-EOB-DTPA-enhanced MRI between April 2008 and February 2011. These patients met the following criteria: (i) positive for HCV RNA or HBsAg; (ii) negative for antinuclear antibodies or antimitochondrial antibodies in the serum, as determined by radioimmunoassay or spot hybridization; and (iii) no history of treatment with corticosteroids, immunosuppressants or antiviral agents. Among these patients, laparoscopy-guided liver biopsy was performed in 52 hepatitis B patients and 57 hepatitis C patients; the other 49 hepatitis B patients and 195 hepatitis C patients were diagnosed with liver cirrhosis clinically. These 244 clinically diagnosed cirrhotic patients were classified into Child–Pugh class A–C according to clinical data. Table 1 summarizes the patients' characteristics. All patients diagnosed with stage F4 fibrosis by histology were classified as Child–Pugh class A. This study was approved by the Institutional Review Board of our hospital. Written informed consent was obtained from all patients.

Laparoscopy

Laparoscopy-guided liver biopsy was performed in 52 hepatitis B patients and 57 hepatitis C patients between April 2008 and February 2011. Details of the procedures of laparoscopy and laparoscopic biopsy were described previously.[32] Based on the irregularities of the liver surface, the laparoscopic findings were classified into three groups: (i) smooth (smooth liver surface or with limited areas of depression); (ii) irregular (the liver surface showed increased numbers of interconnected depressions, possibly resembling ripples or specks); and (iii) nodular (liver surface with nodular formations) as reported in our previous study.[32] The physicians in charge explained the purpose and method of the laparoscopy-guided liver biopsy to each patient, who gave their informed consent for participation. The criterion of laparoscopic diagnosis of liver cirrhosis was the demonstration of multiple nodular irregularities on the liver surface.

Histopathological evaluation

Liver biopsy specimens were obtained using a modified Vim Silverman needle of 2 mm internal diameter (Tohoku University style, Kakinuma Factory, Tokyo, Japan), fixed in 10% formalin, and stained with hematoxylin–eosin, Masson-trichrome, silver impregnation, and periodic acid-Schiff after diastase digestion. Each specimen used for examination contained more than six portal areas. Histopathological interpretation of

Table 1 Characteristics of included patients ($n = 353$)

Characteristic	Value		
	Hepatitis B virus ($n = 101$)	Hepatitis C virus ($n = 252$)	All ($n = 353$)
Median age (years)	52 (range 23–71)	62 (37–86)	58 (23–86)
Sex (male/female)	70/31	148/104	218/135
Histological diagnosis (METAVIR)			
F1	13	5	18
F2	10	14	24
F3	13	12	25
F4	16	26	42
Clinical diagnosis			
Child–Pugh A	42	101	143
Child–Pugh B	5	72	77
Child–Pugh C	2	22	24

the specimens was made by experienced liver pathologists who were blinded to the clinical information. Liver fibrosis was evaluated semiquantitatively according to the METAVIR scoring system.[18] Fibrosis was staged on a 0–4 scale (F0, no fibrosis; F1, portal fibrosis without septa; F2, portal fibrosis and few septa; F3, numerous septa without cirrhosis; F4, cirrhosis).

Viral markers of HCV and HBV

The diagnosis of HCV infection was based on the detection of serum anti-HCV antibodies and positive RNA. Anti-HCV antibodies were tested by the second-generation enzyme-linked immunosorbent assay (Abbott Laboratories, North Chicago, IL). HCV RNA was measured by the Amplicor method (Cobas Amplicor HCV Monitor test ver. 2.0; Roche Diagnostic Systems, Tokyo, Japan). HBsAg was tested by radioimmunoassay (Abbott Laboratories).

MRL

Multiple resonance imaging was obtained from all patients with a 1.5-T MRI system (Avanto, Siemens-Asahi Meditec, Tokyo, Japan) using a phased-array coil for signal detection. All patients underwent transverse 3-D of the liver with fat suppression (volumetric interpolated breath-hold examination [VIBE]) sequence in a single breath hold (18–20 s) at hepatobiliary phase of 20 min after injection of the contrast medium. Breathing was withheld at exhalation. The contrast medium used was Gd-EOB-DTPA (Primovist; Bayer Schering Pharma, Berlin, Germany) at a dose of 0.025 mmol/kg bodyweight (0.1 mL/kg). The MRI parameters were: TR, 4.3 msec; TE, 2.1 msec; flip angle, 15°; parallel imaging factor 2 (GRAPPA); slice thickness, 1.5 mm; matrix, 192 × 320; and field of view, 360 mm. 3-D reconstructions of the liver were rendered with enhanced MRI data using ZIOSTAION (Zio software, Tokyo, Japan). Various structures around the liver on the 3-D image were marked manually and then cut and removed digitally. Finally, the liver was extracted on the workstation. The following findings were noted on MRL: (i) irregular liver surface; (ii) impression of the right ribs; (iii) enlargement of the lateral segment; and (iv) atrophy of the right lobe. The MRL findings of the liver surface were classified into three categories: (i) smooth (essentially smooth surface of the entire liver or with limited areas of depression); (ii) partially irregular (several interconnected depressions on the surface mainly in the left lobe of the liver, with rippled or speckled appearance); and (iii) diffusely irregular (nodules present on the liver surface). The patient with diffusely irregular liver surface was diagnosed as liver cirrhosis.

Statistical analysis

All statistical analyses were performed using the Statistical Package for Social Sciences software (SPSS, Chicago, IL, USA).

RESULTS

MRL of the normal liver

FIGURE 1 SHOWS the MRL images of the normal liver. The liver surface irregularities in patients with normal liver were classified as smooth ($n = 48$) and partially irregular ($n = 1$), and none showed diffuse

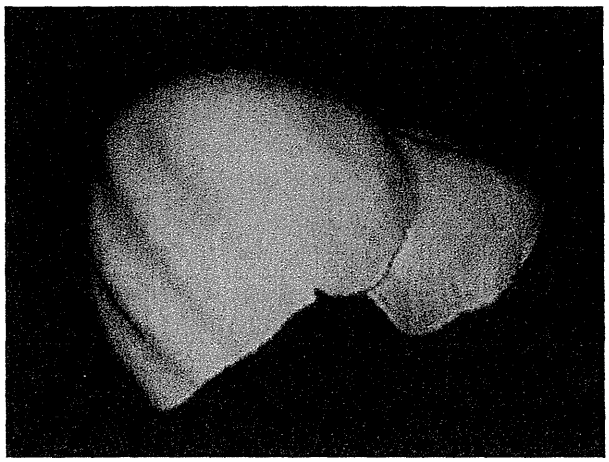

Figure 1 The image of normal liver by magnetic resonance laparoscopy: (i) irregularity of liver surface, smooth; (ii) impression of the right ribs, positive; (iii) enlargement of the lateral segment, negative; and (iv) atrophy of the right lobe, negative.

irregular pattern. Impression of the right ribs on the liver was observed in all patients. None of the patients showed enlargement of the lateral segment or atrophy of the right lobe.

Comparison of biopsy, laparoscopy and MRL

Figure 2(a–c) shows laparoscopic images and MRL image of a representative patient with chronic hepatitis C and fibrosis of F1 stage. The surface findings were well reproduced on the MRL images compared with laparoscopy. Although observation of the liver surface was restricted on laparoscopy, the entire liver surface was visualized on MRL. The correlation between laparoscopic, MRL and histological findings are shown in Table 2. The liver surface patterns on laparoscopy were distributed as follows: smooth, $n = 13$; irregular, $n = 20$; and nodular, $n = 19$. The liver surface patterns on MRL were distributed as follows in patients with HBV: smooth, $n = 14$; partially irregular, $n = 18$; and nodular, $n = 20$. The liver surface patterns on laparoscopy were distributed as follows: smooth, $n = 5$; irregular, $n = 25$; and nodular, $n = 27$. The liver surface patterns on MRL were distributed as follows in patients

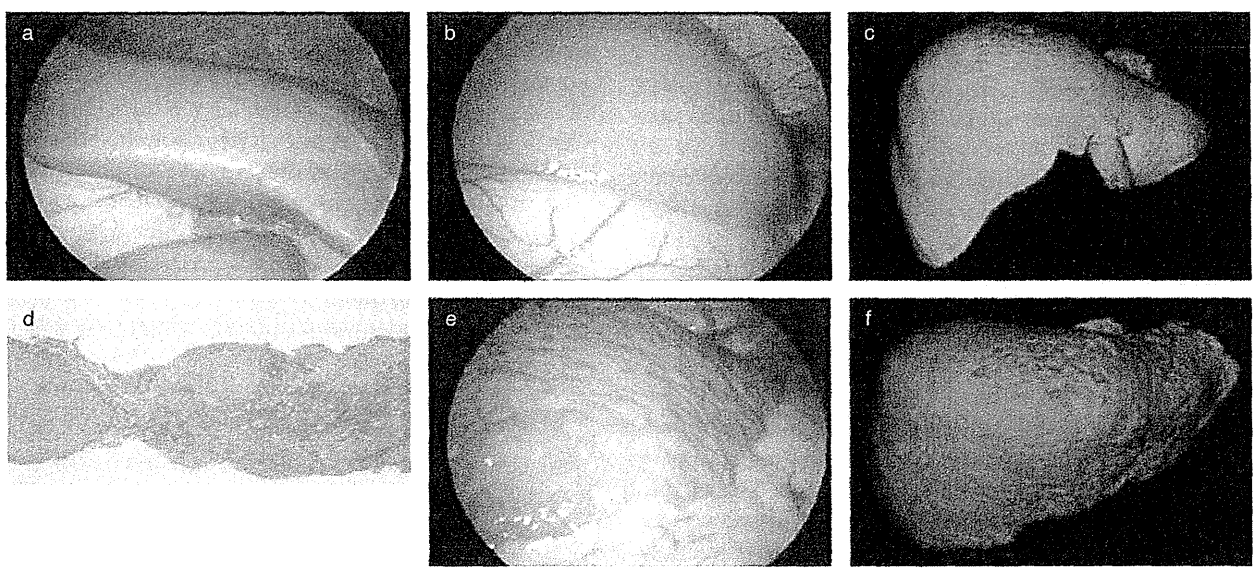

Figure 2 Comparison of laparoscopy, magnetic resonance laparoscopy (MRL) and biopsy. (a–c) Chronic hepatitis C with METAVIR score of F1 examined by laparoscopy and MRL. (a,b) The liver surface was smooth on laparoscopy. (c) On MRL: (i) irregularity of the liver surface, smooth; (ii) impression of the right ribs, positive; (iii) enlargement of the lateral segment, positive; and (iv) atrophy of the right lobe, negative. (d–f) Liver cirrhosis with hepatitis B virus infection. (d) Needle biopsy findings included numerous septa without cirrhosis, indicative of score F3 (hematoxylin-eosin staining, original magnification ×100). (e) Examination by laparoscopy showed nodular liver surface, confirming the diagnosis of cirrhosis. (f) Examination by MRL showed the following features: (i) irregularity of the liver, diffuse irregular; (ii) impression of the right ribs, negative; (iii) enlargement of the lateral segment, positive; and (iv) atrophy of the right lobe, negative.

Table 2 Comparison of laparoscopic, multiple resonance laparoscopic and histological findings

Hepatitis B virus patients ($n = 52$)				
Surface findings of multiple resonance laparoscopy	Surface findings of laparoscopy			
	n	Smooth ($n = 13$)	Irregular ($n = 20$)	Nodular ($n = 19$)
Smooth	14	12	2	0
Partial irregular	18	1	17	0
Diffuse irregular (nodular)	20	0	1	19
Histological findings (METAVIR)	Surface findings of laparoscopy			
	n	Smooth ($n = 13$)	Irregular ($n = 20$)	Nodular ($n = 19$)
F1	13	11	2	0
F2	10	2	8	0
F3	13	0	10	3
F4	16	0	0	16
Hepatitis C virus patients ($n = 57$)				
Surface findings of multiple resonance laparoscopy	Surface findings of laparoscopy			
	n	Smooth ($n = 5$)	Irregular ($n = 25$)	Nodular ($n = 27$)
Smooth	8	5	3	0
Partial irregular	23	0	22	1
Diffuse irregular (Nodular)	26	0	0	26
Histological findings (METAVIR)	Surface findings of laparoscopy			
	n	Smooth ($n = 5$)	Irregular ($n = 25$)	Nodular ($n = 27$)
F1	5	4	1	0
F2	14	1	13	0
F3	12	0	11	1
F4	26	0	0	26

with HCV: smooth, $n = 8$; partially irregular, $n = 23$; and nodular, $n = 26$. There were close similarities in liver surface findings between laparoscopic and MRL. Based on the surface findings on laparoscopy, the sensitivity, specificity, positive predictive value and negative predictive value for the diagnosis of cirrhosis by MRL were 96%, 100%, 95% and 95%, respectively. In comparison, the respective values were 86%, 98%, 97% and 91%, respectively, for the diagnosis by histological examination. These results indicate that MRL is more accurate than needle biopsy in the diagnosis of cirrhosis.

Changes in MRL findings with progression of liver fibrosis

Table 3 lists changes in MRL findings with disease progression. Liver surface irregularities increased with the progression of liver damage. The impression of the right ribs was observed in all livers including normal livers and those with chronic hepatitis. The incidence of impression of the right ribs decreased in patients with cirrhosis classified as Child–Pugh A. Furthermore, the impression of the right ribs disappeared in cases with advanced cirrhosis, namely, patients classified clinically as Child–Pugh B and C. The enlargement of the lateral segment was observed in chronic hepatitis with F2 grade fibrosis and more severe fibrosis. Atrophy of the right lobe was observed in patients with cirrhosis. The incidence of atrophy of the right lobe increased with the progression of Child–Pugh classification. All patients with F4 grade fibrosis were classified as Child–Pugh A, and the proportion of MRL findings was similar in the F4 group and clinically diagnosed group of Child–Pugh A. Figure 3 shows the MRL images for each histopathological and clinical stage, including changes in the liver surface.

Table 3 Proportion of liver surface findings of multiple resonance laparoscopy according to histological and clinical stage

	Irregularities of liver surface			Impression of the right ribs	Enlargement of the lateral segment	Atrophy of the right lobe
	Smooth	Partial irregular	Diffuse irregular (Nodular)			
Hepatitis B virus patients ($n = 101$)						
Histological diagnosis (METAVIR)						
F1 ($n = 13$)	92% (12/13)	8% (1/13)	0% (0/13)	100% (13/13)	46% (6/13)	0% (0/13)
F2 ($n = 10$)	20% (2/10)	80% (8/10)	0% (0/10)	100% (10/10)	90% (9/10)	0% (0/10)
F3 ($n = 13$)	0% (0/13)	69% (9/13)	31% (4/13)	100% (13/13)	100% (13/13)	0% (0/13)
F4 ($n = 16$)	0% (0/16)	0% (0/16)	100% (16/16)	88% (14/16)	100% (16/16)	19% (3/16)
Clinical diagnosis						
Child–Pugh A ($n = 42$)	0% (0/42)	0% (0/42)	100% (42/42)	74% (31/42)	100% (42/42)	19% (8/42)
Child–Pugh B ($n = 5$)	0% (0/5)	0% (0/5)	100% (5/5)	20% (1/5)	40% (2/5)	80% (4/5)
Child–Pugh C ($n = 2$)	0% (0/2)	0% (0/2)	100% (2/2)	0% (0/2)	0% (0/2)	100% (2/2)
HCV patients ($n = 252$)						
Histological diagnosis (METAVIR)						
F1 ($n = 5$)	100% (5/5)	0% (0/5)	0% (0/5)	100% (5/5)	0% (0/5)	0% (0/5)
F2 ($n = 14$)	21% (3/14)	79% (11/14)	0% (0/14)	100% (14/14)	86% (12/14)	0% (0/14)
F3 ($n = 12$)	0% (0/12)	92% (11/12)	8% (1/12)	100% (12/12)	100% (0/12)	0% (0/12)
F4 ($n = 26$)	0% (0/26)	4% (1/26)	96% (25/26)	85% (22/26)	100% (0/26)	12% (3/26)
Clinical diagnosis						
Child–Pugh A ($n = 101$)	0% (0/101)	9% (9/101)	91% (92/101)	83% (84/101)	100% (101/101)	13% (13/101)
Child–Pugh B ($n = 72$)	0% (0/72)	0% (0/72)	100% (72/72)	7% (5/72)	97% (70/72)	96% (69/72)
Child–Pugh C ($n = 22$)	0% (0/22)	0% (0/22)	100% (22/22)	0% (0/22)	45% (10/22)	100% (22/22)

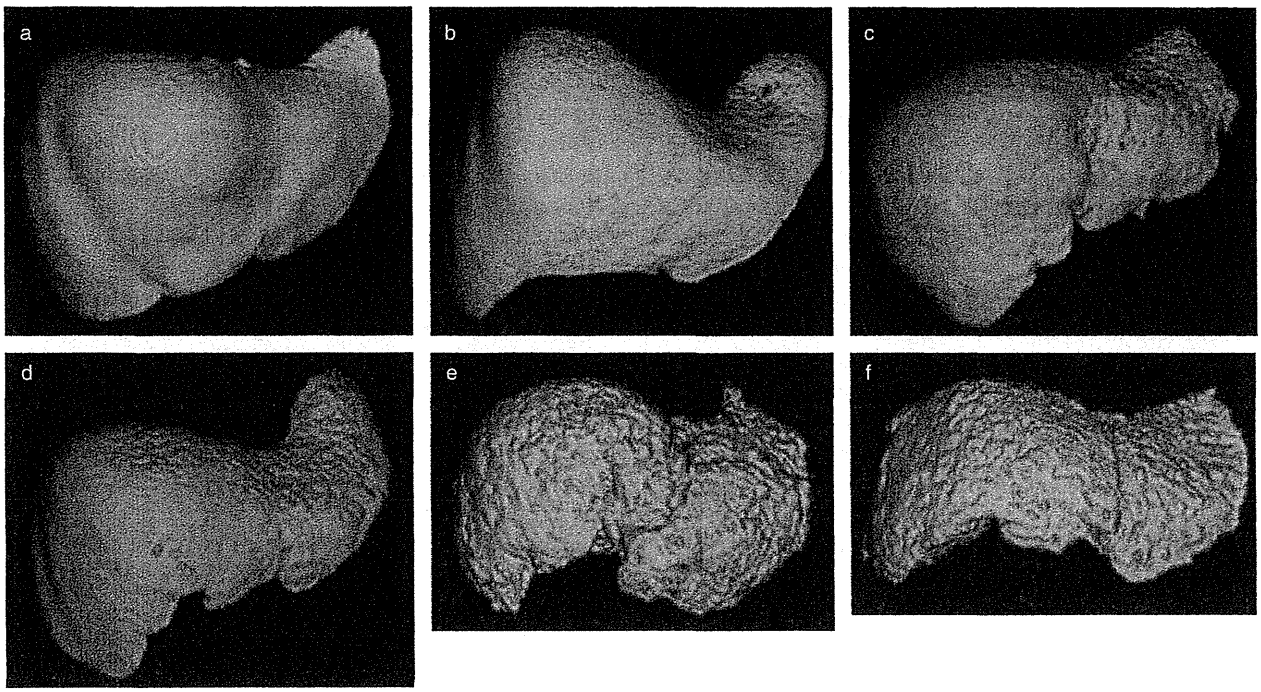

Figure 3 Magnetic resonance laparoscopy images of different stages of liver fibrosis. (a) METAVIR score F1, (b) METAVIR score F2, (c) METAVIR score F3, (d) cirrhosis, Child–Pugh A, (e) cirrhosis, Child–Pugh B, (f) cirrhosis, Child-Pugh C.

Comparison of MRL findings in patients with HBV and HCV

Table 3 shows proportion of liver surface findings of MRL in each stage of fibrosis which was diagnosed by histological examination. Diffuse irregular pattern was not observed in both HCV and HBV patients with F1 and F2 stage fibrosis. But in HBV patients with F3 stage fibrosis, higher proportion of diffuse irregular pattern was observed compare to HCV patients with F3 stage fibrosis. Almost all liver cirrhosis patients showed diffuse irregular pattern in MRL. In general, the MRL findings were almost similar in HBV- and HCV-related chronic liver disease.

DISCUSSION

ORLANDO *ET AL.* reported that evaluation of both laparoscopy and liver biopsy was useful. In his study, when the two techniques were considered separately, a final diagnosis of cirrhosis was possible in 78.4% by laparoscopy and in 78.8% by biopsy, whereas, doing both procedures improved the diagnostic yield to 97.7% by decreasing the percentage of false negatives for each technique.[36] Wetzke-Braun *et al.* also reported that diagnostic laparoscopy was more accurate than liver biopsy in recognizing cirrhosis in patients with chronic hepatitis C.[12] These results suggest that laparoscopic examination of the liver is superior for the diagnosis of liver cirrhosis compared with liver biopsy. In this study, comparison of MRL and liver biopsy in the diagnosis of liver cirrhosis showed sensitivity, specificity, positive predictive value and negative predictive value of 96% versus 86%, 100% versus 98%, 95% versus 97% and 95% versus 91%, respectively. Furthermore, the surface findings on MRL could be stratified according to the laparoscopic findings (Table 2). These results suggested MRL could evaluate the surface findings of liver in the same way as laparoscopy.

However, liver biopsy is currently considered as the gold standard for assessing liver fibrosis, this procedure has certain problems, though it is in general a safe procedure. It is an invasive technique with a morbidity rate of 3% and mortality rate of 0.003%.[15,16] In addition, liver biopsy examination carries intra- and interobserver variability in the staging of liver fibrosis, with sampling error mainly due to the small size of the harvested specimen, which represents at most 1/50 000 of the entire liver mass.[17–19] In this study, 19 HBV patients and 27